

# Photoluminescence Study of Rare Earth Doped ZnO Nanoparticles

P.K. Upadhyay<sup>1</sup>, A. K. Shrivastav<sup>2</sup>, Shashank Sharma<sup>3</sup>, Ravi Sharma<sup>4\*</sup>

<sup>1</sup> Department of Physics, Govt. Nagrik Kalyan Mahavidyalaya Ahiwara, Durg (C.G.) India

<sup>2</sup> Physics Department, Dr C. V. Raman University, Kargi road kota, Bilaspur (C.G.) India

<sup>3</sup> Mechanical Department, University College of Engineering, Osmania University, Hyderabad, India

<sup>4\*</sup> Physics Department, Govt. Devendra Nagar Girls College Raipur (C.G.) India

\*\*\*

**Abstract:** ZnO nanoparticles are synthesized by the chemical route using thiourea as organic capping agent. The effect doping of rare earth ion on photoluminescence, optical and on structural property of ZnO nanoparticle are analyzed. The growth of nano ZnO was confirmed by X-ray diffraction (XRD), Scanning Electron Microscope (SEM). The non spherical morphology of nano ZnO could be seen by the Scanning Electron Microscope photographs. The particle sizes of nanoparticles were calculated experimentally using XRD and SEM. The particle size measured by XRD pattern was found to be 56nm for doped sample, whereas, it was 66 nm for undoped sample. SEM images showed no any particular structure and showed agglomeration of nanoparticles. The band gap calculated from the absorption spectra was ~4.32 eV for the undoped sample and for rare earth doped ZnO nanoparticles it was ~4.28 eV. The PL excitation spectra showed three peaks at 392nm, 416nm and 464nm and the emission spectra showed three peaks at 596nm, 646 and 736 nm, showing the characteristic peaks of Eu<sup>3+</sup> ions for the doped sample.

**Keywords:** Pholuminescence, XRD Characterization, ZnO nanoparticles, Rare earth.

## Introduction

Nanomaterials play a very important role in today's material world. The nanomaterials exhibit unique and different physical, chemical and biological properties when compared to their macro scaled counterparts [1]. In the last few decades, inorganic nanoparticles, whose structures showed significantly new and improved physical, chemical, and biological properties and functionality due to their nano size was much studied. Several types of inorganic metal oxides like TiO<sub>2</sub>, ZnS and ZnO were studied for their optical, magnetic and electronic properties that can be easily tuned by changing the morphology. ZnO seems to be a promising contender, and the development of this phosphor could make a massive impact technologically worldwide. ZnO NPs are of maximum interest, among the metal oxide, because they are inexpensive to produce, safe and can be prepared easily, having high stability and environment friendly material. Zinc oxide nanoparticles belong to the class of metal oxides, which is characterized by photocatalytic and photo-oxidizing capacity against chemical and biological species [2]. ZnO nanoparticles have been used in light-emitting devices (LEDs), improvement of power conversion efficiency of solar energy, gas sensors, intense room temperature luminescence electronics, communication, sensor, cosmetics, environmental protection, for biological sensing, biological labelling, gene delivery, drug delivery and nanomedicines etc [3-13]. Since ZnO semiconductor can be easily nanostructured, its optical properties can also be tuned at nanosize scale because of high quantum confinement effects.

Presently, the foremost materials of interest are rare earth (RE) based phosphors. Rare-earths ion doping has been adopted in order to increase the lifetime of charge carriers and subsequently reduce the recombination probability [14]. Rare earth ions are ideal candidates for spectral conversion, because of their  $f \rightarrow f$  or  $f \rightarrow d$  internal orbital transitions that give very intense emission lines with high luminescence efficiencies and rich energy level structure that allows for great flexibility in the upconversion and downconversion of photons in a wide spectral region [15-17]. It has been revealed theoretically that europium (Eu<sup>3+</sup>) showed great potential as a dopant in ZnO because it exhibits sharp emission in both the UV and visible range, making it as a suitable candidate for fiber lasers, plasma displays, solar cells and bio-imaging and in field emission display devices in general [18-20].

Many synthesis methods have been used to produce nanostructured ZnO such as nanoneedles, nanonails, nanobelts, nanorods and nanobowls. The conventional physical and chemical methods that have been used for the synthesis of ZnO nanoparticles are chemical vapor synthesis, laser ablation, solvothermal and sol-gel method, co-precipitation and combustion method [21-25]. However, these methods are usually expensive, labor-intensive, and are potentially hazardous to the environment and living organisms. By controlling parameters such as temperature, mixing rate, dopant concentrations, degree of alkalinity and

pH of the reaction materials with high purity and fine particle size at relatively moderate cost could be made [26, 27]. In present study, we have synthesized samples of ZnO nanoparticles by wet chemical method. The structural characterization by XRD, SEM and optical characterization by UV-VIS spectrometry was made. The synthesized nanoparticles produced by both methods have different size and morphology. Photoluminescence (PL) studies were carried out on the Eu doped ZnO powder phosphors. The absorption, excitation and emission properties of these phosphors were also recorded.

### Experimental

Zinc acetate ( $\text{Zn}(\text{CH}_3\text{COO})_2 \cdot 2\text{H}_2\text{O}$ ), thiourea ( $(\text{NH}_2)_2\text{CS}$ ) and ammonia (25%  $\text{NH}_3$ ) was used as the starting materials, for the preparation of the ZnO samples. The samples were prepared by dissolving zinc acetate, thiourea and ammonia in deionised water, separately. The chemical bath technique was used. Zinc acetate, thiourea and ammonia solutions were mixed at ratio of 1:1:1 and rapidly heated to 80°C stirring it continuously. The prepared ZnO nanoparticles were washed with acetone, ethanol and deionized water. All the reagents of AR-grade were used without further purification.

The morphologies and sizes of as prepared ZnO nanoparticles were determined by X-ray diffraction using  $\text{Cu K}\alpha$  radiation ( $\lambda = 1.5418 \text{ \AA}$ ). Rigaku Rotating Anode (H-3R) diffractometer was used for X-ray diffraction patterns. XRD data were collected over the range  $2\theta - 70^\circ$  at room temperature. For scanning electron microscope (SEM), JSM - 5,600 LV was used. Absorption spectra of the samples prepared was recorded with the help of Perkin Elmer Model Lamda 950 UV-VIS spectrophotometer. For PL measurements Perkin Elmer spectrofluorophotometer Model LS 45 was used.

### Results and Discussions

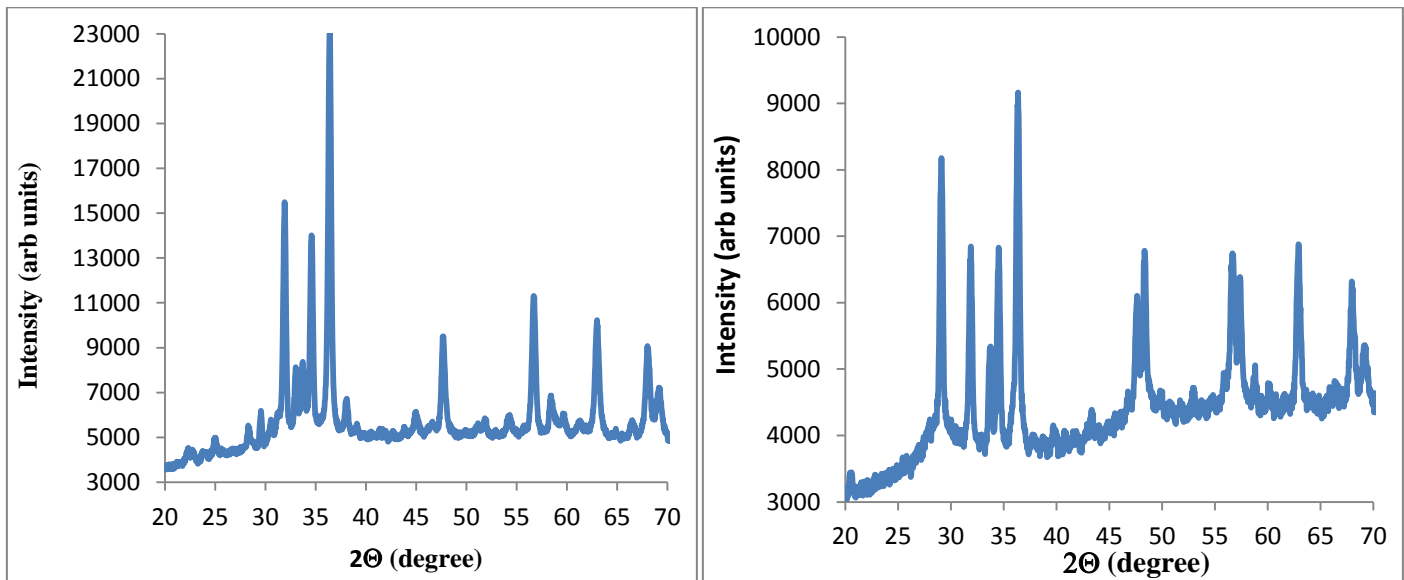


**Fig.1a XRD of undoped ZnO nanoparticl Fig.1b XRD of rare earth doped ZnO nanoparticle**

The crystal structure and purity of ZnO nanoparticles were characterized by X- ray diffraction (XRD) studies. Figure 1a shows the XRD pattern of the undoped ZnO nanoparticles synthesized by chemical method. From the above figure it could be inferred that the synthesized ZnO nanoparticles are in pure phase, i.e. no impurities are seen in the XRD pattern. The peaks obtained at  $2\theta^\circ$  values of 31.62, 34.33, 36.12, 47.33, 56.31, 62.64, 66.03, 67.64, and 68.73 can be attributed to the planes (100), (002), (101), (102), (110), (103), (200) and (112), (201) respectively. All the peaks are in good agreement with hexagonal wurtzite structure of ZnO well matched with standard data (JCPDS 36-1451). Broadening in the XRD peaks could be seen very clearly, which confirms the nanocrystalline nature of zinc oxide. Fig.1b shows XRD pattern of rare earth ( $\text{Eu}^{3+}$ ) doped ZnO nanoparticles. Broad diffraction peaks were observed with one extra peak attributed to plane (001) obtained at  $2\theta^\circ$  value of 27.82 was observed. Few more peaks adjacent to already present peaks at 47.33, 56.31 are also clearly visible. Rest all other peak are slightly shifted towards lower angle side, which may be due to doping of rare earth ion or increasing lattice strain and inter planar spacing [28, 29]. The broadening occurs in all the peaks. This is due to the smaller particle size and large number

of crystal planes present in the sample. This broadening in turn causes a loss of intensity in the signal of their diffraction patterns.

For both the samples the average crystallite size was determined from the XRD pattern parameters using Debye Scherrer equation  $D = k\lambda / \Delta \cos \theta$ , where D is the average crystallite size, k is Scherrer's constant equal to 0.90,  $\Delta$  is the full-width at half-maximum (FWHM), and  $\theta$  is the Bragg's angle [30]. The strain-induced broadening in powders due to crystal imperfection and distortion was calculated using the formula  $\epsilon = \Delta \tan \theta$  [31].

Table 1

Samples	Lattice Parameter ( $\text{\AA}$ )		d spacing	Lattice Strain	Cristallite Size
	a	c			
Undoped	3.132 $\text{\AA}$	5.188 $\text{\AA}$	2.4672	0.1681	66nm
Rare earth doped	3.143 $\text{\AA}$	5.168 $\text{\AA}$	2.4443	0.1978	56nm

Table 1 shows the lattice parameter, crystallite size, d-spacing and lattice strain of ZnO nanoparticles for undoped and rare earth doped samples. The crystallite size for undoped synthesized ZnO was found to be 66nm, whereas, the size of rare earth doped ZnO was found 56nm.

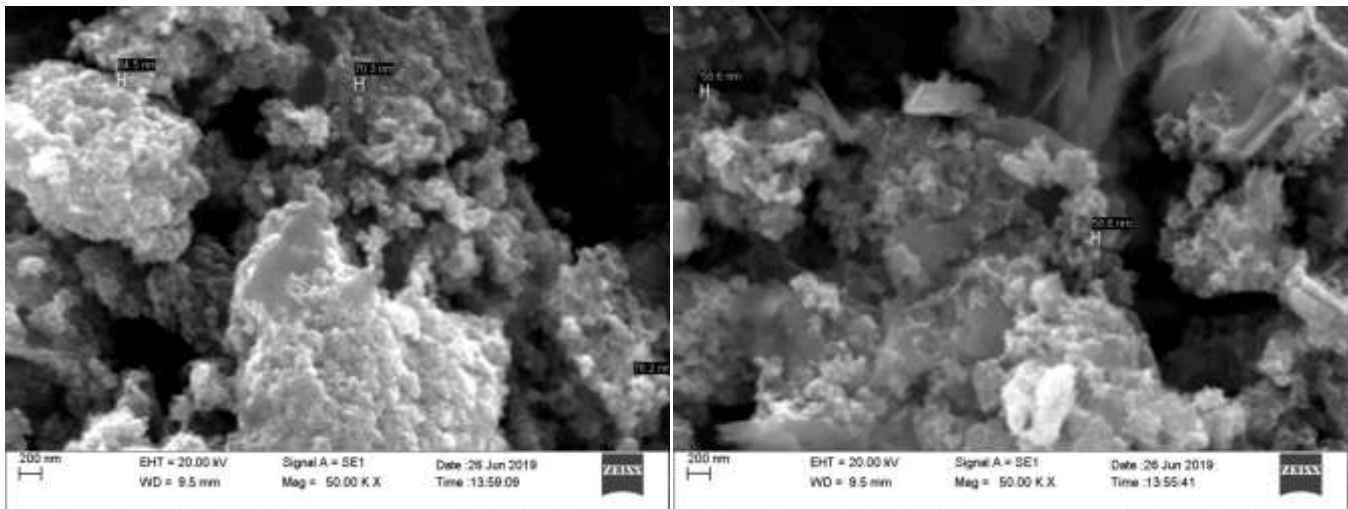


Fig. 2a SEM of undoped nano ZnO Fig. 2b SEM of rare earth doped nano ZnO

The morphologies of synthesized ZnO nanoparticles were investigated by scanning electron microscopy. Figure 2 (a&b) shows the SEM image of undoped and rare earth doped ZnO nanoparticles synthesized by chemical method respectively. For both the samples no any special structure could be seen. It can be seen that many of the particles are agglomerated, this is due to the formation of ZnO nanoparticles during first few minute of the experiment and later these particles agglomerates and their size becomes larger. The average particle sizes obtained from SEM images was ~ 69 nm. The SEM patterns agree well with the XRD results. In the figure 2(b), highly agglomeration of particles is clearly seen. The average size of these synthesized non spherical powder ZnO nanoparticles is ~ 58.6 nm. Many of the particles are in the range less than 50nm. The hexagonal structure is not clearly visible for both the samples.

The UV-visible absorption spectra of undoped and rare earth doped ZnO nanoparticles synthesized by chemical method as a function of wavelength is shown in Figure 3. In both the cases, the absorption band shows a blue shift as compared to bulk due to the quantum confinement effect [32]. Figure 3 shows that the optical absorption spectra of the nano ZnO measured between 240 nm- 400 nm. It was found that the spectra are featureless and very less absorption occurred in the visible region. The absorption peak for the undoped nano ZnO by chemical method was recorded at 277nm. The absorption peak of rare earth doped ZnO nanoparticle was found at 272 nm, which lies much below the band gap wavelength of 388 nm of bulk ZnO [33].

The peak at ~272 nm is due to inter band transition of electrons from the more inner shell to the uppermost shell. It is possible that, due to aggregation and agglomeration, particle size increases and material settled down at the bottom of container causing decrease in the absorbance [34]. This type of behavior is typical for many semiconductors due to internal electric fields within the crystal and inelastic scattering of charge carriers by phonons [35, 36].

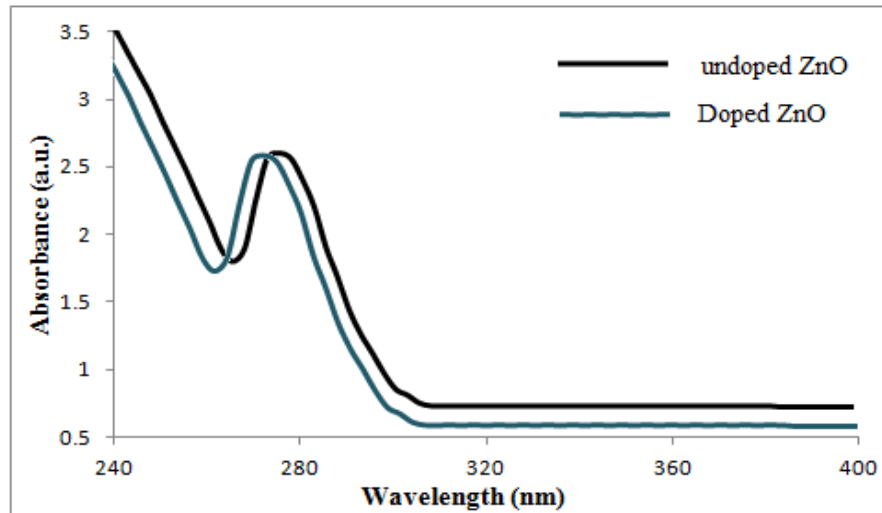
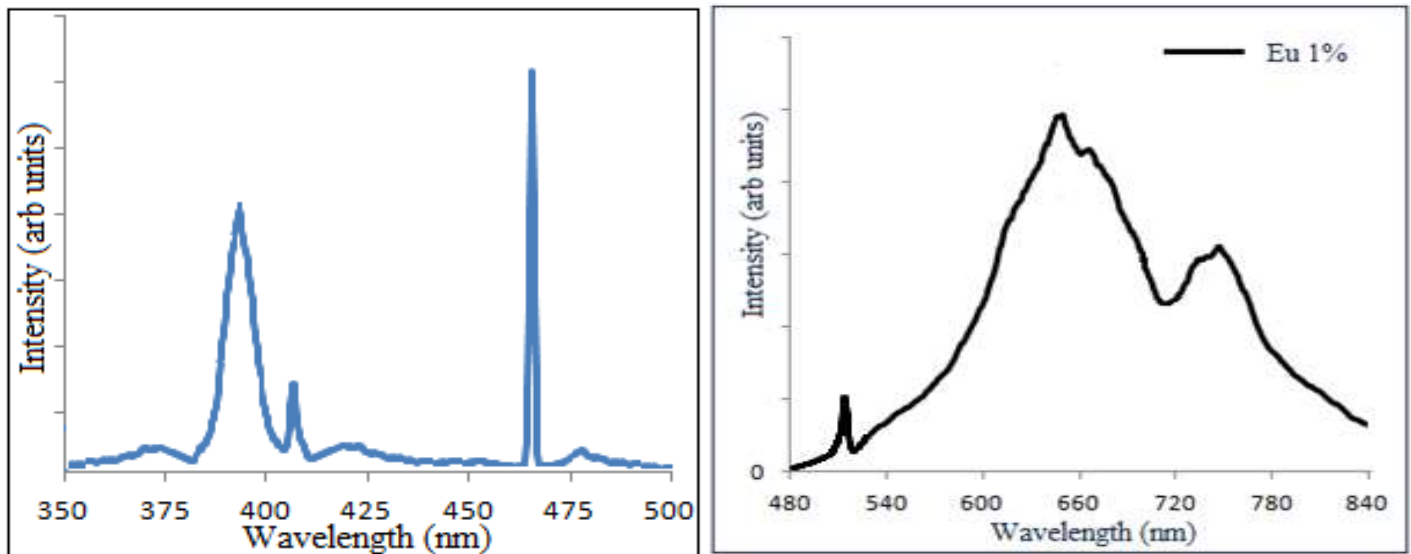


Fig. 3 Absorption spectra of undoped and rare earth doped ZnO nanoparticles

Absorption coefficient ( $\alpha = 2.303A/t$ ) of nano ZnO were calculated from absorbance (A) and the sample thickness (t). The optical band gap of ZnO nanoparticles is calculated using the Tauc relation:  $\alpha h\nu = \alpha_0(h\nu - E_g)^n$ , Where,  $\alpha$  is the absorption coefficient,  $h\nu$  is the energy of incident photons and exponents  $n$  whose value depends upon the type the transition.. The band gap calculated from the above data was ~4.32 eV for the undoped sample and for rare earth doped ZnO nanoparticles it was ~4.28 eV, which is higher than reported value 3.54 eV. The increase in the band gap of the ZnO nanoparticles with the decrease in particle size may be due to a quantum confinement effect. This is an indication that the capping agent played an important role in controlling the particle size.

Study of the photoluminescence (PL) is an interesting property of material that can provide valuable information on the quality of the material. Luminescence studies provide information regarding defect states. PL studies may reveal the shift in defect states or the change in the density. Fig. 5 displays the PL spectra of the  $\text{Eu}^{3+}$  doped ZnO nanopowder recorded at room temperature using monochromatized xenon lamp as excitation source. Fig. 5(a) shows the excitation spectra of  $\text{Eu}^{3+}$  doped ZnO nanoparticle with emission wavelength 646 nm and 5(b) the emission spectra of  $\text{Eu}^{3+}$  doped ZnO nanoparticle with excitation wavelength 460 nm. The excitation spectrum of the undoped sample shows a steep absorption around 392 nm which correspond to the ZnO band gap, while the  $\text{Eu}^{3+}$  doped ZnO samples exhibited sharp lines at 416 nm and 464 nm, which are due to the 4f-4f intrinsic transitions of  $\text{Eu}^{3+}$  in ZnO. The sharp lines at 416 nm and 464 nm were associated with the  ${}^7F_0 - {}^5L_6$  and  ${}^7F_0 - {}^5D_2$  transitions of  $\text{Eu}^{3+}$  respectively. The emission spectrum of the  $\text{Eu}^{3+}$  doped ZnO nanoparticle shows the characteristic emissions of  $\text{Eu}^{3+}$  at 596 nm, 646 nm and 736 nm, which are due to  ${}^5D_0 - {}^7F_1$ ,  ${}^5D_0 - {}^7F_3$  and  ${}^5D_0 - {}^7F_4$  transitions, respectively. The emission arising from the electric dipole transition is higher than the emission from the magnetic dipole transition, which indicates that the  $\text{Eu}^{3+}$  ions occupy sites without inversion symmetry. According to Blasse theory, resonant transfer by exchange interaction or multipole- multipole interaction is responsible for the non-radiative energy transfer of the luminescence [37].



(a) Excitation spectra (b) Emission spectra

**Fig.5 Photoluminescence spectra of  $\text{Eu}^{3+}$  doped ZnO nanoparticles**

## Conclusions

The nanoparticles of ZnO have been successfully synthesized by a simple chemical reaction using aqueous medium; in which thiourea was used as the capping agent. The XRD pattern indicated the growth of the ZnO nanoparticles in hexagonal phase. The crystallite size measured by XRD pattern was found to be 66nm for chemically synthesized undoped ZnO nanoparticle and 56nm for rare earth doped ( $\text{Eu}^{3+}$ ) ZnO sample. SEM images do not show any particular shape or structure but agglomerated ZnO nanoparticles. The SEM photograph also shows that the particle sizes are bigger for undoped samples. The band gap calculated from the absorption spectra data was  $\sim 4.32$  eV for the undoped sample and for rare earth doped ZnO nanoparticles it was  $\sim 4.28$  eV. The solid-state theory based on the delocalized electron and hole within the confined volume explains the blue-shifted optical absorption spectra. The PL excitation spectra showed three peaks at 392nm corresponding to the band gap of ZnO, and 416nm and 464nm which are due to the 4f-4f intrinsic transitions of  $\text{Eu}^{3+}$  in ZnO. The emission spectra showed three peaks at 596nm, 646 and 736 nm, showing the characteristic peaks of  $\text{Eu}^{3+}$  ions for the doped sample which are due to  ${}^5\text{D}_0 - {}^7\text{F}_1$ ,  ${}^5\text{D}_0 - {}^7\text{F}_3$  and  ${}^5\text{D}_0 - {}^7\text{F}_4$  transitions, respectively.

## References

- [1] S. Chaturvedi, Pragnesh N. Dave, N.K. Shah, J Saudi Chem Soc. 16, 3, 307 -325, (2012)
- [2] Deepali Sharma JR, Kaith BS, Kaur Mohinder, Sharma Sapna, Thin Solid Films 519:1224–1229, (2010)
- [3] Hussein J, El-Banna M, Razik TA, El-Nagga ME, Int J Biol Macromol. <https://doi.org/10.1016/j.ijbio mac.2017.09.056>, (2017)
- [4] Wang L, Kang Y, Liu X, Zhang S, Huang W, Wang S, Sens Actuators B: Chem 162:237–243, (2012)
- [5] Cross SE, Innes B, Roberts MS, Tsuzuki T, Robertson TA, McCormick P Human, Skin Pharmacol Physiol 20:148–154, (2007)
- [6] A. Umar, R. Kumar, G. Kumar, H. Algarni, S.H. Kim, J. Alloys Compd. 648 46–52, (2015).
- [7] K.P. Raj, K. Sadayandi, Physica B 487, 1–7, (2016).
- [8] K.Q. Le, H.P.T. Nguyen, Q.M. Ngo, A. Canimoglu, N. Can, J. Alloys Compd. 669, 246–253, (2016).
- [9] F. Lu, W. Cai, Y. Zhang, Adv. Funct. Mater. 18, 1047–1056, (2008).
- [10] S. Sabir, M. Arshad, S.K. Chaudhari, Sci. World J. 2014, 1–8 (2014).

- [11] Zhou J, Xua N, Wang ZL, Adv Mater 18:2432–2435, (2006).
- [12] Rasmussen JW, Martinez E, Louka P, Wingett DG, Exp Opin Drug Deliv 7:1063–1077, (2010).
- [13] Shaheen TI, El-Naggar ME, Abdelgawad AM, Hebeish A, Int J Biol Macromol. <https://doi.org/10.1016/j.ijbiomac.2015.11.003>, (2015).
- [14] A. Khataee, A. Karimi, M. Zarei, S.W. Joo, Ultrason. Sonochem, 30, 1-9, (2015)
- [15] Andries Meijerink, online, 04 February 2013,
- [16] Vinod Kumar, S. Som, Vijay Kumar, Vinay Kumar, O.M. Ntwaeaborwa, E. Coetsee, H.C. Swart, Chem. Eng. J. 255, 541–552, (2014).
- [17] R. Zamiria, A.F. Lemos, A. Rebloa, H.A. Ahangar, J.M.F. Ferreira, Ceram. Int. 40, 523–529, (2014).
- [18] M. Chndrasekhar, H. Nagabhushana, Y. SVIDYA, K.S. Anantharaju, S.C. Sharma, H.B. Premkumar, S.C. Prashantha, B.D. Prashantha, B.D. Prasad, C. Shivakumara, R. Saraf, H.P. Nagaswapura, J. Mol. Catal. A 409, 26–41, (2015).
- [19] N. Yao, J. Huang, K. Fu, X. Deng, M. Ding, M. Shao, X. Xu, Electrochim. Acta 154, 273–277, (2015).
- [20] L.R. Singh, Mater. Sci. Appl. 6, 269–278, (2015).
- [21] Lobiak, E.V., Shlyakhova, E.V., Bulusheva, L.G., Plyusnin, P.E., Shubin, Yu.V. and Okotrub, A.V., Journal of Alloys and Compounds, 621, 351-356, (2015).
- [22] Cho, J.M., Song, J.K. and Park, S.M., Bulletin of the Korean Chemical Society, 30, 1616-1618, (2009).
- [23] Wang, C., Shen, E., Wang, E., Gao, L., Kang, Z., Tian, C., Lan, Y. and Zhang, C., Current Applied Physics, 6, 499-502, (2006).
- [24] Hasnidawani, J.N., Azlina, H.N., Norita, H., Bonnia, N.N., Ratim, S. and Ali, E.S., Procedia Chemistry, 19, 211-216, (2016).
- [25] V. Mangalam, K. Pita, C. Couteau, Nanoscale Res. Lett. 11, 73, (2016).
- [26] G. Vijayaprasath, R. Murugan, T. Mahalingam, Y. Hayakawac, G. Ravi, Ceram. Int. 41, 10607–10615, (2015).
- [27] A. Pachtak, P. Pramanik, PINSA, 67, 47–70, (2001).
- [28] S. Kumar, K. Asokan, R. K. Singh, S. Chatterjee, D. Kanjilal and A. K. Ghosh, RSC Adv., 4, 62123 -62131, (2014).
- [29] P. Bindu, Sabu Thomas, J. Theor. Appl. Phys., 8, 123 – 134, (2014).
- [30] R. Sharma, S.J. Dhoble, D.P. Bisen, N. Brahme, B.P. Chandra, Int. J. Nanoparticles 4 (1), 64 – 76, (2011)
- [31] Songül Fiat Varol, Göknil Babür, Gökten Ankaya and Uğur Kölemen, RSC Adv., 4, 56645 -56653, (2014).
- [32] Huang, M.H.; Mao, S.; Feick, H.; Yan, H.; Wu, Y.; Kind, H.; Weber, E.; Russo, R.; Yang, P.D, Science, 292, 1897–1899, (2001).
- [33] Pathik Kumbhakar, Devendra Singh, Chandra S. Tiwary, Amya K. Mitra, Chalcogenide letters 5, 387-394, (2008).
- [34] T. S. Moss, G. J. Burrell, B. Ellis, Semiconductor Opto-Electronics, Butterworth & Co. Ltd. 1973.
- [35] H. M. Honsi, S. A. Fayek, S. M. Al-Sayed, M. Roushdy, M. A. Soliman, Vacuum 81, 54-58, (2006).
- [36] A. Sawby, M. S. Selim, S. Y. Marzouk, M. A. Mostafa, A. Hosny, Physica B: Physics of Condensed Matter 405, 3412-3420, (2010).
- [37] G. Blasse, Concentration quenching of Eua+ fluorescence, J. Chem. Phys. 46, 2583, (1967).